Applied Clay Science 146 (2017) 70–80

Contents lists available at ScienceDirect

Applied Clay Science

journal homepage: www.elsevier.com/locate/clay

Research paper

Mullite-zirconia composites prepared from halloysite reaction sintered with boehmite and zirconia

A. Raghdi[a], M. Heraiz[a], F. Sahnoune[a], N. Saheb[b,*]

[a] Physics and Chemistry of Materials Lab, Department of Physics, University Mohamed Boudiaf of M'sila, 28000 M'sila, Algeria
[b] Department of Mechanical Engineering, King Fahd University of Petroleum and Minerals, Dhahran 31261, Saudi Arabia

ARTICLE INFO

Keywords:
Clay minerals
Halloysite
Gibbsite
Boehmite
Reaction sintering
Mullite-zirconia composites

ABSTRACT

In this study, Algerian halloysite, a naturally occurring clay mineral, was used as low-cost precursor for the production of mullite-zirconia composites. The halloysite was reaction sintered with boehmite and zirconia in the temperature range 1250–1650 °C for 2 h. Differential thermal analysis (DTA), thermogravimetry (TG), dilatometry, high temperature X-ray diffraction (XRD), and scanning electron microscopy (SEM) complementary techniques were used to characterize the prepared materials. The influence of ZrO_2 content on the microstructure, densification, hardness, and coefficient of linear thermal expansion of the composites was investigated. Algerian halloysite was found suitable material for the synthesis of low-cost mullite based composites. All prepared samples exhibited same phase transformations that ended at 1550 °C with the formation of monolithic mullite in halloysite-boehmite mixture and mullite-zirconia composites in halloysite-boehmite-zirconia mixture. The composite materials showed higher values of hardness and coefficient of linear thermal expansion compared with monolithic mullite. The composite containing 10% ZrO_2 possessed the highest hardness value of 13.5 GPa. The composite containing 30% ZrO_2 possessed the lowest value of linear coefficient of thermal expansion of $7.5725 \times 10^{-6} K^{-1}$ between 200 and 1500 °C.

1. Introduction

The occurrence of mullite in nature is so rare because it is the result of reaction between alumino-silicate minerals at high temperatures (Manfredini and Manuskova, 2012). Fortunately, low-cost mullite and mullite based advanced ceramics can be easily produced by simple heat treatment of clay minerals such as kaolinite (Sahnoune et al., 2008a,b) and halloysite (Harabi et al., 2014). Mullite is an attractive advanced ceramic material for structural and functional applications because of its excellent thermal, optical, and mechanical properties as well as stability under severe environments (Heraiz et al., 2013). However, the low fracture toughness of mullite limited its wide use in many applications (Rezaie et al., 1999). As a result, a second phase such as zirconia is usually added to mullite to produce composites that have improved properties (Sahnoune et al., 2011). Over the past years, researchers used various starting raw materials and different processing methods to synthesize mullite-zirconia composites (Schneider et al., 1994; Park et al., 2005; Belhouchet et al., 2007, 2009). Because of its low cost, reaction sintering remained the most attractive method for the preparation of mullite containing ceramic matrix composites. In this process, chemical reaction between the starting minerals and/or raw materials as well as densification have been attained in a one-step simple heat treatment (Yangyun and Brook, 1985). This inexpensive method was used to prepare mullite based ceramics (Alves et al., 2016, 2017) as well as mullite-alumina (Heraiz et al., 2013), zirconia-mullite (Chandra et al., 2015), and alumina-mullite (Medeiros et al., 2016) composites.

Alves et al. (2016) synthesized mullite based ceramics by reactive sintering of kaolin clay and kaolin waste mixtures. They reported the formation of mullite and glass phases in kaolin waste processed ceramics sintered at 1550 °C. In another study, Alves et al. (2017) followed a low-cost preparation method to synthesize mullite-based ceramics by reaction sintering kaolin and 25 wt% mica-rich kaolin waste. They reported the formation of mullite containing 1.2 wt% quartz after firing at 1500 °C. Algerian kaolin and boehmite were found suitable raw materials for the synthesis of Al_2O_3 containing mullite through reaction sintering (Heraiz et al., 2013). Chandra et al. (2015) prepared dense zirconia-mullite composites by reaction sintering zircon flour and reactive alumina with different proportions of MgO and CaO additives. They concluded that MgO facilitated the formation of mullite and zirconia. In another work, alumina-mullite composites were prepared via reactive sintering of a mixture of kaolinite clay mineral

* Corresponding author.
E-mail address: nouari@kfupm.edu.sa (N. Saheb).

http://dx.doi.org/10.1016/j.clay.2017.05.037
Received 27 February 2017; Received in revised form 23 May 2017; Accepted 25 May 2017

and aluminum hydroxide (Medeiros et al., 2016). The authors demonstrated the possibility of preparing low cost alumina-mullite composites with technological properties compatible with those of ceramics produced by companies with large operations in the international market of refractory products.

Furthermore, many researchers successfully synthesized mullite-zirconia composites via reaction sintering different starting materials. These include zircon and alumina mixtures (Torrecillas et al., 1993), Indian coastal zircon flour and calcined alumina with addition of yttria (Das et al., 1998), alumina, amorphous silica with the addition of stabilized zirconia (Lin, 1999), zircon and alumina derived from the oxidation of Al between 1200 and 1600 °C (Ebadzadeh, 2005), alumina and zircon powders together with acicular aluminum borate templates (Öztürk and Tür, 2007), alumina and zircon (Rendtorff et al., 2008), gibbsite, boehmite, and zircon powders (Belhouchet et al., 2009), zircon-alumina mixture (Ashrafi et al., 2015), and zircon, kaolinite and alumina mixtures with the addition of 7 wt% of colemanite (Aydın and Gören, 2016).

Halloysite "is a low-cost, natural material having many interesting properties that allow for versatile potential uses in a variety of domains e.g. as filler in polymers, carrier for the loading and controlled release of guest molecules, adsorbent for pollution remediation, and for the synthesis of functional materials" (Joussein et al., 2005; Yuan et al., 2015). Treated Algerian halloysite has been used as Pb(II) adsorbents (Kadi et al., 2012) and crystal violet adsorbents (Belkassa et al., 2013; Mahrez et al., 2015) from aqueous phases. In addition, it was found useful in removing copper(II) ions from aqueous solutions (Mellouk et al., 2009) and dyes from wastewaters (Bessaha et al., 2016). Algerian halloysite was also used to fabricate resistant porous membrane by solid-state reaction (Harabi et al., 2014). Traditionally, halloysites had been used as an alternative raw material to kaolinite for the production of ceramics (Churchman et al., 2016). Algerian kaolinite had been successfully used to synthesize mullite through reaction sintering it with high purity alumina (Sahnoune et al., 2008a,b). In addition, mullite-zirconia composites were produced by reaction sintering Algerian kaolin, α-Al_2O_3, and stabilized zirconia (3Y-TZP) (Sahnoune et al., 2010); and phase transformations in these composites had been investigated (Sahnoune et al., 2011). The objective of this work was to explore the possibility of using Algerian halloysite to synthesize low-cost millite-zirconia composites. The procedure involves heating pure gibbsite in air to obtain boehmite (Cesteros et al., 1999; Digne et al., 2002), and then reaction sintering Algerian halloysite with boehmite and zirconia to produce millite-zirconia composites. Complementary techniques were used to characterize and analyze phase transformations and sintering behavior. Additionally, the influence of ZrO_2 content on the microstructure, densification, hardness, and coefficient of linear thermal expansion of the composites was investigated.

2. Materials and methods

2.1. Starting materials

Algerian holloysite, a natural raw material from Djabal Debagh (Guelma, East Algeria), aluminum hydroxide ($Al(OH)_3$) obtained from VWR International S.A.S., and zirconium dioxide (ZrO_2) supplied by Biochem chemopharma, Georgia-USA, were used in this investigation. The gibbsite (aluminum hydroxide) was heat-treated at 400 °C to obtain boehmite (α-aluminum oxyhydroxide, α-AlOOH). Gibbsite and boehmite are the most common aluminum hydroxide and oxyhydroxide minerals in nature (Gitzen, 1970). They play important roles in the preparation of high purity alumina. In this work, boehmite was used as a source of alumina.

2.2. Processing of powders

The holloysite, boehmite, and zirconia were mixed to obtain 100/00 (wt%), 90/10, 80/20, 75/25, and 70/30 mullite/ZrO_2 composites, and were named HB00Z, HB10Z and HB20Z, HB25Z, and HB30Z, respectively. Each mixture "was charged into zirconia vials (250 ml in volume) together with 15 zirconia balls (10 mm in diameter), and water was added to the mixture at a ratio of 2:1. The ball milling experiments were performed in a high-energy planetary ball mill (Fritsch P6) and were carried out at room temperature at a rotation speed of 250 rev/min. The milled mixture was dried at 150 °C for 24 hours then compacted at a pressure of 75 MPa using a cold uniaxial press to produce cylindrical specimens of 13 mm diameter" (Sahnoune et al., 2008a,b, 2011). The compacted samples were reaction sintered in the temperature range 1250–1650 °C for 2 h.

2.3. Characterization and analysis

TG and DTA experiments were carried out using a LABSYS EVO DTA/DSC-TG SETARAM equipment. Dilatometry experiments were performed on unfired mixtures as well as samples sintered at 1600 °C for 2 h, using NETZSCH (Dil 402 C) equipment. TG/DTA and dilatometry experiments were performed from room temperature to 1600 °C using heating rates of 20 and 5 °C/min, respectively. A high-temperature diffractometer MRD, PANalytical (ISM), with CuKα radiation of a wavelength 0.15418 nm was used to characterize the raw powders as well as sintered samples. The bulk density of samples was measured by water immersion method using a KERN densimeter. Morphology of the halloysite powder and the microstructure of sintered samples were characterized using a JEOL scanning electron microscope (SEM) model JSM-7001F. A universal hardness-testing machine (Zwick-Roell, ZHV, Germany) was used to measure the Vickers hardness of the sintered samples. Conditions of a load of 500 g and a dwell time of 10 s were used.

The magnitude of the Vickers hardness was determined according to:

$$H_v = 1.854\frac{P}{d^2}$$

where P is the applied load (in N) and d is the diagonal length (in mm). Values for the reported hardness were the average of 10 readings.

3. Results and discussion

3.1. Characterization of raw materials

Typical scanning electron micrographs and particle size distribution of the halloysite powder are presented in Fig. 1. The majority of particles have platy or irregular shapes, Fig 1(a) and (b), respectively. The powder has a wide particle size distribution, Fig. 1(c), and the majority of particles have sizes around 10 and 50 μm. Although the most common reported morphology of halloysite was the elongated tubule and short tubular (Tan et al., 2016), spheroidal and platy particle shapes have all been widely reported (Joussein et al., 2005). The chemical composition of halloysite, $Al_2Si_2O_5(OH)_4$-$2H_2O$, as determined by X-ray fluorescence (XRF) is presented in Table 1. The halloysite contains approximately 44 and 38 wt% of SiO_2 and Al_2O_3, respectively. Other oxides are present in the form of impurities exception CaO.

In halloysite, a dioctahedral 1:1 clay mineral, the alumina octahedral sheet is bound to the silica tetrahedral sheet by covalent bonds, forming layers. "In the formation of the halloysite lattice, hydroxyl groups of one layer are bound to O^{2-} ions of another layer by hydrogen bonds" (Kadi et al., 2012). Halloysite, a polymorph of kaolinite, has similar chemical constitution and crystal structure to kaolinite (Tan et al., 2015). The structural formula of halloysite is $Al_2(OH)_4Si_2O_5{\cdot}nH_2O$, where the value of n is equal to two for hydrated halloysite and zero for dehydrated halloysite (Joussein et al., 2005; Yuan et al., 2015). XRD spectra of raw halloysite and samples treated at

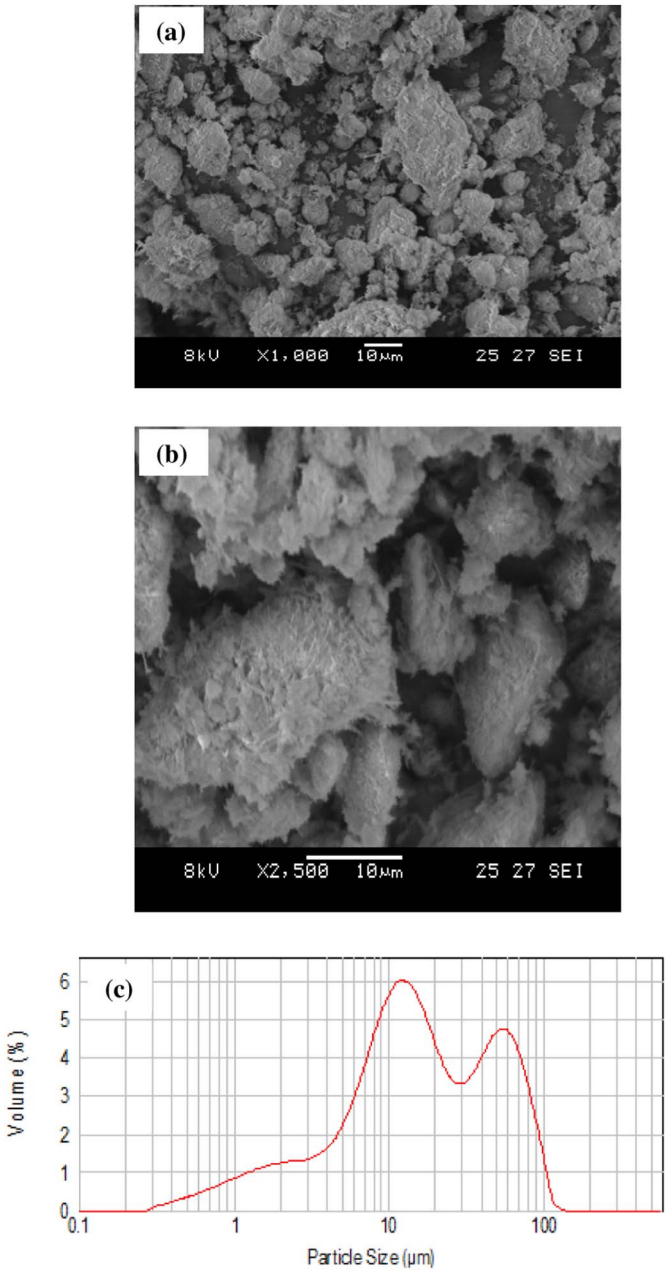

Fig. 1. Raw halloysite (a, b) SEM images and (c) particle size distribution.

Table 1
Chemical composition of halloysite.

Compounds	SiO_2	Al_2O_3	CaO	Fe_2O_3	MgO	SO_3	K_2O	Na_2O
wt%	43.99	38.04	2.07	0.12	0.51	0.09	0.01	0.14

400, 800, and 1200 °C for 2 h are presented in Fig. 2(a). The spectrum of the untreated halloysite showed only reflections characteristic of halloysite-10 Å (Tan et al., 2015). After heating at 400 °C, halloysite -10 Å was converted to halloysite-7 Å. This is due to the loss of the interlayer water (Joussein et al., 2006; Yuan et al., 2012). The spectrum of sample treated at 800 °C showed broad and low intensity diffraction maxima because of dehydroxylation and the formation of amorphous metahalloysite (Smith et al., 1993; Yuan et al., 2012). It was reported that the rearrangement of hydroxylated halloysite leads to the formation γ-alumina and amorphous silica (Kadi et al., 2012). After heating at 1200 °C, only reflections characteristic of mullite, believed to be formed from γ-alumina and amorphous silica, were present. This is in agreement with what reported by Yuan et al. (2012).

TG/DTA curves of halloysite raw powder, heated from room temperature to 1400 °C at a heating rate of 20 °C/min, are presented in Fig. 2(b). Two endothermic peaks at 105 and 556 °C, and three exothermic peaks at 997, 1171, and 1290 °C are present. The first mass loss (about 1 wt%) in the temperature range 57–150 °C is due to the evaporation of adsorbed water corresponding entirely to the first endothermic peak at 105 °C. The second mass loss (about 13 wt%) in the temperature range 400–650 °C is due to the dehydration of the halloysite and the formation of metahalloysite, correlating with the second endothermic peak at 556 °C. This can be described by the equation:

$$Al_2O_3{\cdot}2SiO_2{\cdot}2H_2O \xrightarrow{400^{\circ}C-650^{\circ}C} Al_2O_3{\cdot}2SiO_2 + 2H_2O$$

The 13% mass loss is very close to the theoretical mass loss of 14% calculated from the above reaction (Kadi et al., 2012). The first exothermic peak at 997 °C corresponds to the transformation of metahalloysite to spinel phase and SiO_2. It is worth mentioning here that researchers debated whether the alumina-rich phase formed in this reaction is a spinel-like γ-Al_2O_3 or an alumina-rich mullite (Okada et al., 1986; Brindley and Lemaitre, 1987; Sonuparlak et al., 1987; Yuan et al., 2012). The second exothermic peak observed at 1171 °C is due to the transformation of the spinel phase to primary mullite. The third exothermic peak observed at 1290 °C is due to the crystallization of free silica, which yields a crystalline phase called cristobalite.

XRD spectrum of pure gibbsite i.e. aluminum hydroxide $Al(OH)_3$ is presented in Fig. 3 (a). Upon heating at 400 °C for 2 h, the gibbsite changed to boehmite as confirmed by analysis of XRD spectrum shown in Fig. 3(b). This supports the fact that boehmite (Wang et al., 2009; Rajabi and Derakhshan, 2010), a partially dehydrated aluminum hydroxide, can be produced from aluminum hydroxides by controlled calcination (Day and Hill, 1953; Candela et al., 1986, 1992). The transformation of gibbsite to alumina can be described by the equations (Filho et al., 2016):

$$Al(OH)_3 \xrightarrow{\text{gibbsite to boehmite}} AlO(OH) + 2H_2O$$

$$2AlO(OH) \xrightarrow{\text{boehmite to alumina}} Al_2O_3 + 2H_2O$$

Researchers believed that the formation of boehmite from gibbsite is favored if water vapor formed during heating is retained within the gibbsite particles. This is more possible if, in addition to the pre-existence of water vapor in the system, the gibbsite particles are large and heating rates are high. Otherwise, gibbsite could transform directly to transition γ-alumina (Brindley and Choe, 1961; Wefers and Misra, 1987; Bhattacharya et al., 2004; Filho et al., 2016). Other researcher concluded that gibbsite decomposes to boehmite regardless of the size of its particles (Mercury et al., 2005). Analysis of reflections present on the XRD spectrum, illustrated in Fig. 3(c), confirmed that the boehmite heated at 1200 °C for 2 h transformed to α-Al_2O_3 (Rajabi and Derakhshan, 2010).

Thermal decomposition of gibbsite was also characterized by TG and DTA. Three steps of mass loss were observed on the TG curve depicted in Fig. 3(d). The first mass loss of about 5%, at 210–255 °C, is due to partial transformation of gibbsite to boehmite. The second mass loss of about 23%, attributed to complete transformation of gibbsite to boehmite, starts before the completion of the first and ends approximately at 325 °C corresponding to intense DTG and DTA peaks centered at about 300 °C. The third mass loss, at around 525 °C, corresponding to less intense DTG and DTA peaks, is believed to be due to transformation of boehmite to γ-Al_2O_3 (Filho et al., 2016).

3.2. Phase transformations and sintering behavior

TG/DTA curves of HB30Z sample heated from room temperature to

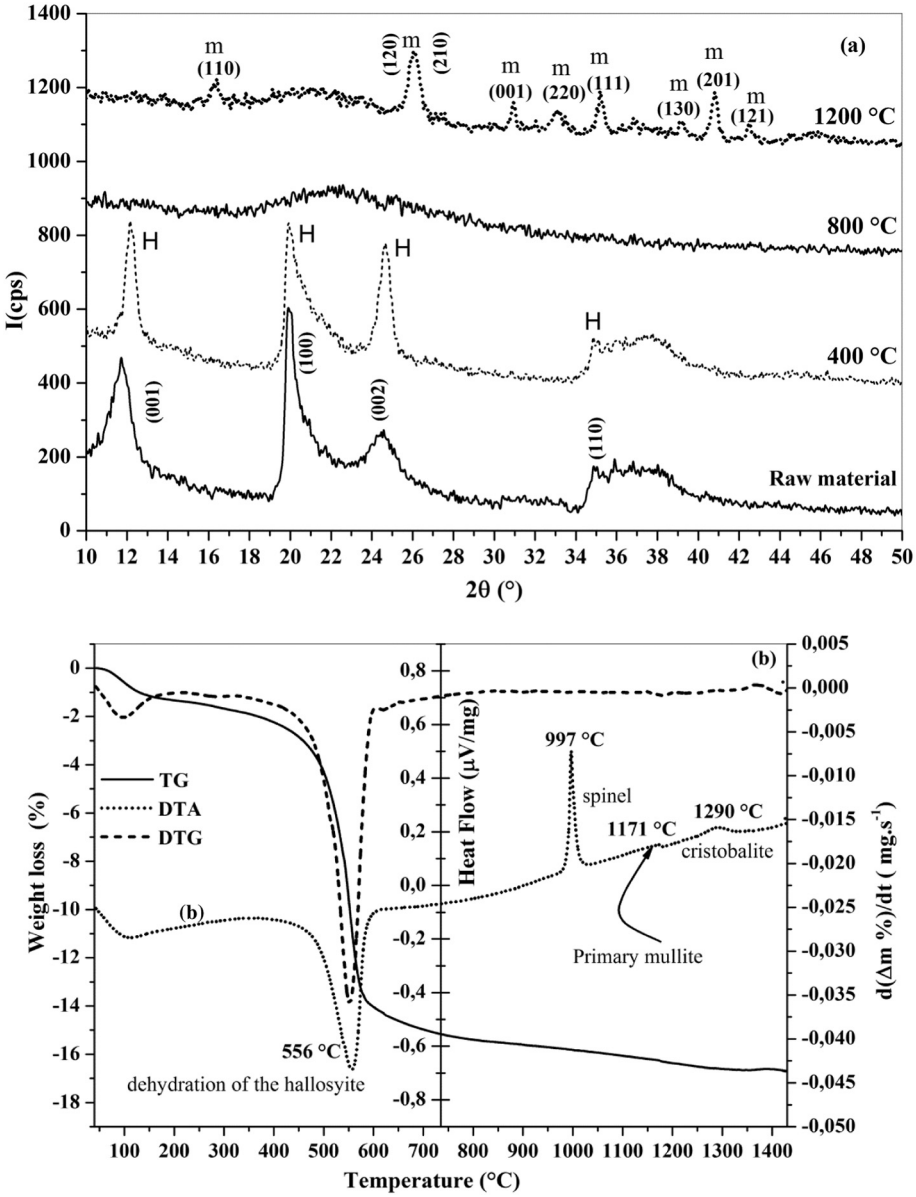

Fig. 2. (a) X-ray diffraction spectra of halloysite treated at different temperatures for 2 h and (b) TG/DTA curves of halloysite heated at 20 °C/min.

1600 °C (heating rate of 20 °C/min) are displayed in Fig. 4. Two endothermic peaks at 105 and 546 °C, and three exothermic peaks at 998, 1153, and 1287 °C are present. The first mass loss (about 1.9 wt%) is due to the evaporation of adsorbed water corresponding entirely to the first endothermic peak at 105 °C. The second mass loss (about 7.8 wt%) in the temperature range 400–650 °C is due to the dehydration of the halloysite and the formation of metahalloysite, correlating with the second endothermic peak at 546 °C. The HB30Z composite and raw halloysite displayed same sintering behavior. This indicates that phase transformations in the composite are mainly governed by the transformation of halloysite.

The mass loss remained constant with heating above 850 °C. The first exothermic peak at 998 °C corresponds to the formation of spinel phase (Al—Si). This value is in agreement with the value of 1006 °C reported by Chen et al. (2004) for the formation of spinel from metakaolinite. In addition, it is close to the values of 984 and 980 °C reported by Sahnoune et al. (2008a,b) and Sonuparlak et al. (1987), respectively, for the formation of spinel from kaolin. The second exothermic peak observed at 1153 °C is due to the formation of primary mullite from the spinel phase. The third exothermic peak observed at 1287 °C is due to the crystallization of free silica, which yields a crystalline phase called cristobalite.

Linear shrinkage curves and their first derivatives obtained from the dilatometry studies performed on unfired halloysite–boehmite and halloysite–boehmite–zirconia samples, between room temperature and 1600 °C at a heating rate of 5 °C/min, are presented in Fig. 5. An expansion was observed at temperature lower that 100 °C due to the evaporation of adsorbed water. The first relative shrinkage started at 467 °C and ended at 636 °C where the rate of shrinkage was maximum at 567 °C. This shrinkage is due to the dehydration of the halloysite which transforms to metahalloysite as follows:

$$Al_2O_3{\cdot}2SiO_2{\cdot}2H_2O + 2Al_2O_3 + xZrO_2 \xrightarrow{567^{\circ}C} Al_2O_3{\cdot}2SiO_2 + 2H_2O\uparrow + xZrO_2$$

A second relative shrinkage started at 950 °C and ended at 1050 °C as a result of the: (i) transformation of metahalloysite to spinel (Al—Si), where the rate of shrinkage was maximum at 980 °C (Pask and Tomsia, 1991; Liu et al., 1994; Sahnoune et al., 2008a,b), and (ii) the transformation of spinel phase (Al—Si) to primary mullite and silica in the form of cristobalite at 1239 °C. This reaction ends at a

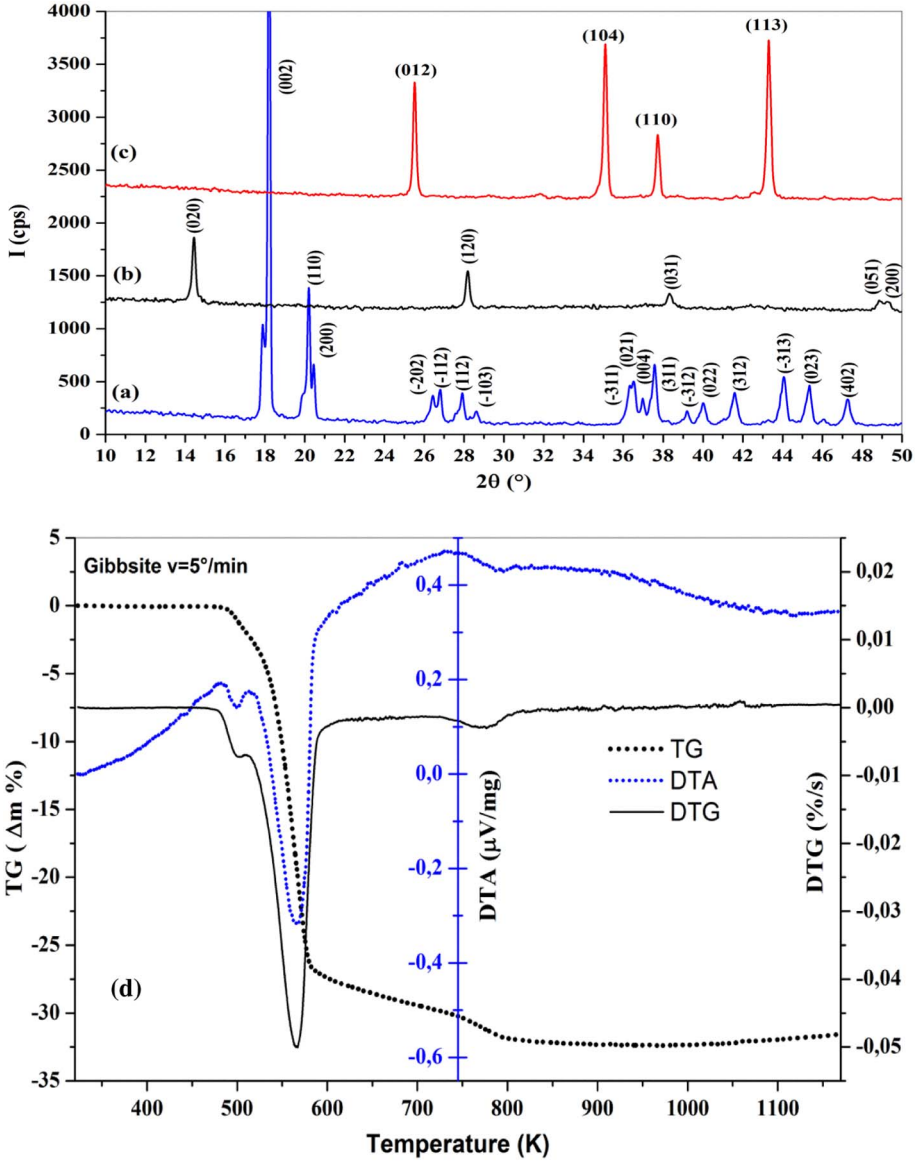

Fig. 3. XRD spectra of (a) gibbsite, (b) boehmite and (c) α-Al_2O_3, and (d) TG/DTA curves of gibbsite heated at 5 °C/min.

temperature lower than 1400 °C and can be described by the equations:

$$Al_2O_3{\cdot}2SiO_2{\cdot}2H_2O + 2Al_2O_3 + xZrO_2 \xrightarrow{980^{\circ}C} \frac{1}{2}(Al_2O_3{\cdot}2SiO_2)(\text{spinel}) + \frac{3}{2}SiO_2(\text{amourphous}) + 2Al_2O_3 + xZrO_2$$

$$\frac{1}{2}(Al_2O_3{\cdot}2SiO_2)(\text{spinel}) + \frac{3}{2}SiO_2(\text{amourphous}) + 2Al_2O_3 + xZrO_2 \xrightarrow{1239^{\circ}C} \frac{1}{3}(3Al_2O_3{\cdot}2SiO_2) + \frac{4}{3}SiO_2 + 2Al_2O_3 + xZrO_2$$

At temperatures higher than 1400 °C, secondary mullite started to form in the halloysite–boehmite sample and completed at 1500 °C. However, for halloysite–boehmite–zirconia samples, other shrinkages took places, which were associated with transformations between 1354 and 1460 °C. The rate of shrinkage was maximum at 1412 °C, which corresponds to the formation of zircon ($ZrSiO_4$) from the reaction between free silica and zirconia (Ramani et al., 1969) as follows:

$$\frac{1}{3}(3Al_2O_3{\cdot}2SiO_2) + \frac{4}{3}SiO_2 + 2Al_2O_3 + xZrO_2 \xrightarrow{1412^{\circ}C} \frac{1}{3}(3Al_2O_3{\cdot}2SiO_2) + 2Al_2O_3 + yZrSiO_4 + \left(\frac{4}{3} - y\right)SiO_2 + (x - y)ZrO_2$$

In the last stage, secondary mullite formed, at a temperature lower than 1501 °C, from the reaction between silica, which resulted from the dissociation of zircon, with the alumina formed from the transformation of boehmite. This led to the formation of mullite in the halloysite–-boehmite sample and mullite–zirconia composite in the halloysite–-boehmite–zirconia samples according to the following equation:

$$\frac{1}{3}(3Al_2O_3{\cdot}2SiO_2) + 2Al_2O_3 + yZrSiO_4 + \left(\frac{4}{3} - y\right)SiO_2 + (x - y)ZrO_2 \xrightarrow{1501^{\circ}C} (3Al_2O_3{\cdot}2SiO_2) + xZrO_2$$

Typical XRD spectra of HB00Z and HB20Z samples sintered between 1250 and 1650 °C for 2 h are illustrated in Fig. 6 (a) and (b). Primary mullite started to form from the spinel phase at 1250 °C. This supports the results of DTA and dilatometry discussed above. Analysis of reflections which appeared at 1350 °C and disappeared at 1500 °C, in

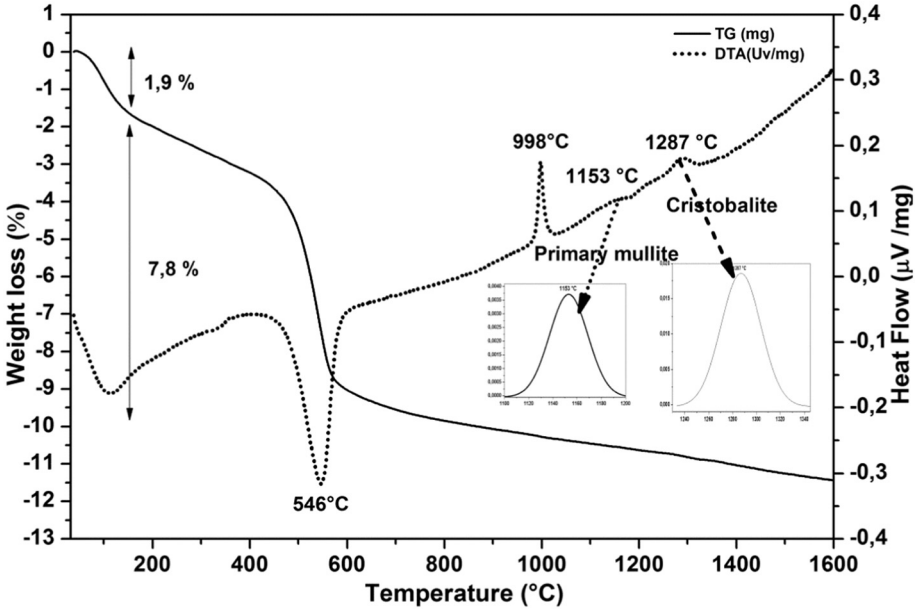

Fig. 4. TG and DTA curves of HB30Z sample heated at 20 °C/min.

both samples, revealed that these reflections are due to the formation of cristobalite through crystallization of free silica, while the alumina reflections remained unchanged. The decrease in the intensity of alumina and cristobalite reflections observed at 1450 °C indicates the beginning of the reaction between the two phases, which leads to formation of mullite and increase in the intensity of its reflections. This transformation ended at 1500 °C for the HB00Z sample. For the HB20Z sample, new reflections started to appear at 1350 °C and became clear at 1400 °C, while the intensity of cristobalite reflections decreased and the intensity of alumina reflections remained unchanged. This is due to the reaction between zirconia (ZrO_2) and silica (SiO_2) and the formation of zircon ($ZrSiO_4$). The later dissociated again to zirconia and silica at 1550 °C (Sahnoune et al., 2011). This was followed by the reaction between silica and alumina to form mullite, as it is evident from the decrease in the alumina reflections and the increase in mullite reflections. It is worth mentioning here that zircon is known to form from the reaction between zirconia and free silica between 1300 and 1400 °C (Ramani et al., 1969), and usually dissociates at temperatures higher or lower than 1675 °C in the absence or presence of impurities, respectively (Shi et al., 1997).

At 1600 °C, only reflections of mullite single phase could be observed in HB00Z sample while reflections of mullite and zirconia phases were present in HB20Z sample. XRD spectra of HB00Z, HB10Z, HB20Z, and HB30Z samples, sintered at 1650 °C for 2 h, are presented in Fig. 6. Analysis of these spectra confirmed the following: (i) the absence of alumina and silica reflections in all samples, (ii) the presence of only a single phase i.e. mullite in zirconia free sample, and (iii) the presence of mullite along with zirconia phase in its monoclinic and tetragonal forms in zirconia containing samples. It can be concluded that all samples exhibited same phase transformations and showed similar sintering behavior, which led to the formation of monolithic mullite in HB00Z sample and mullite-zirconia composites in HB10Z, HB20Z, and HB30Z samples.

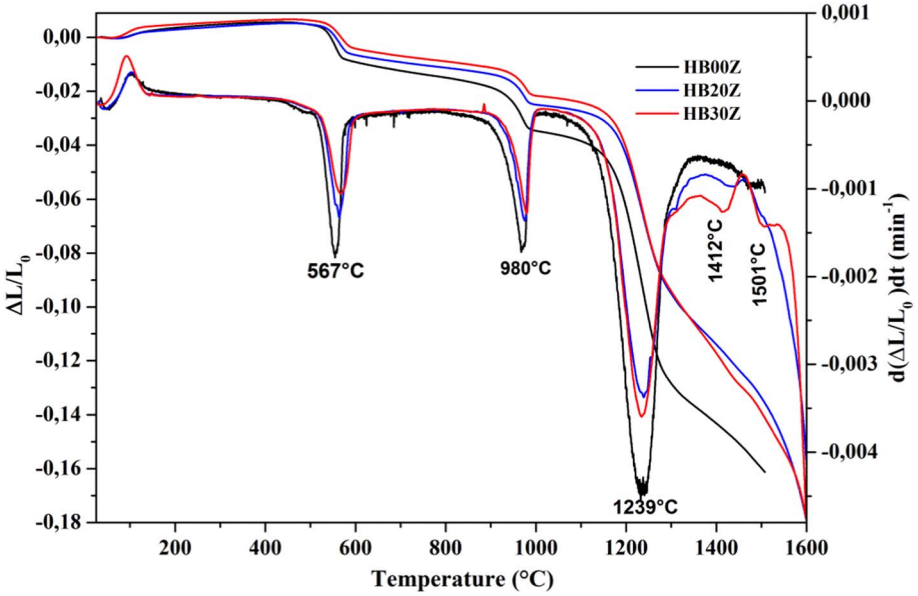

Fig. 5. Dilatometry curves of unfired halloysite-boehmite-zirconia mixtures.

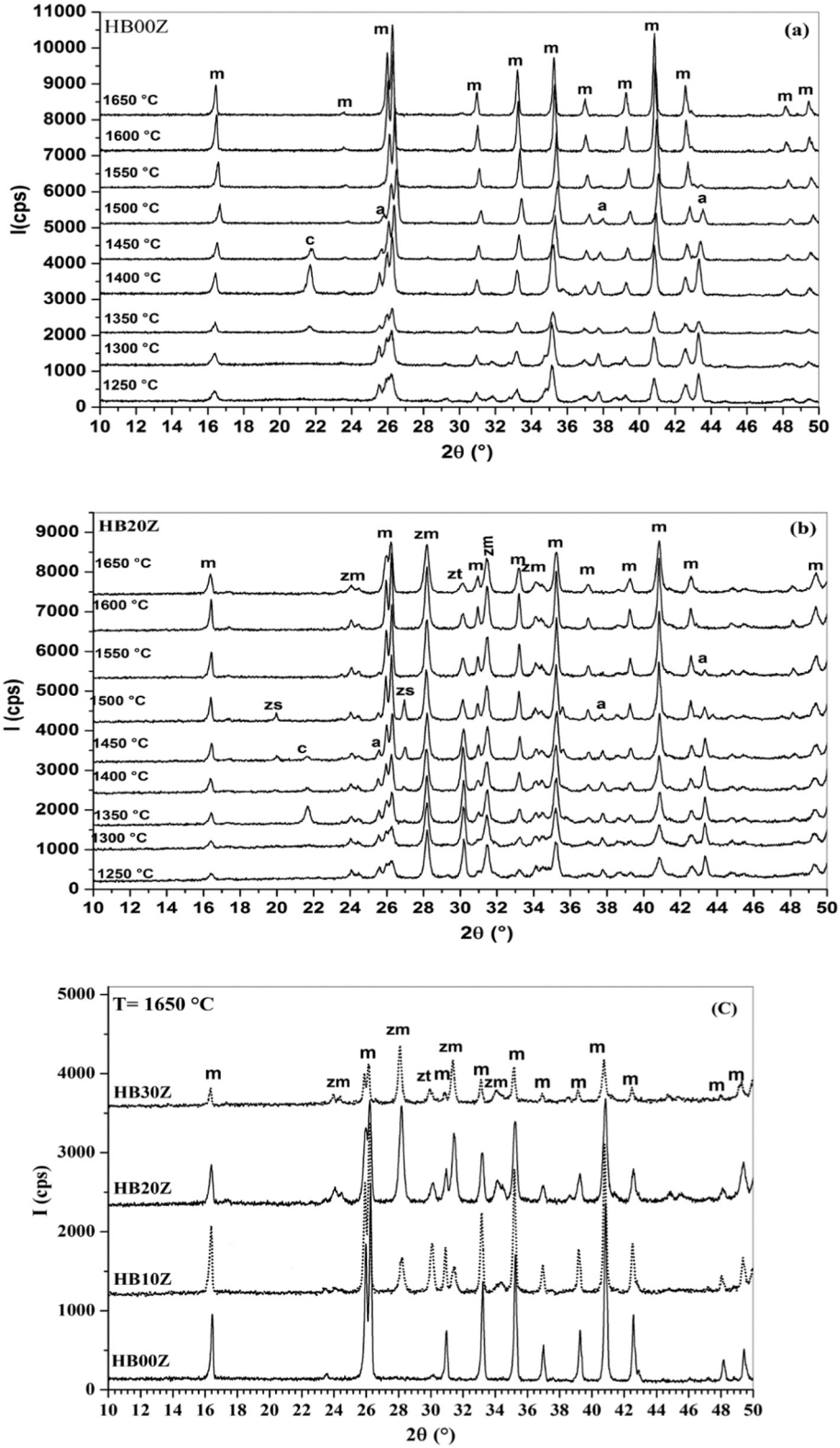

Fig. 6. XRD spectra of (a) HB00Z and (b) HB20Z samples sintered at shown temperatures, and (c) HB00Z, HB10Z, HB20Z and HB30Z samples sintered at 1650 °C for 2 h. (m, mullite; zs, zircon; zm, monoclinic zirconia; zt, tetragonal zirconia; a, α-alumina; and c, cristobalite).

3.3. Densification and microstructure

The change in density of samples sintered at different temperatures, from 1450 to 1650 °C, for 2 h is presented in Fig. 7. The density of all samples decreased with the increase in sintering temperature from 1450 to 1500 °C. For ZrO_2 containing samples, the decrease in density is due to the dissociation of zircon ($ZrSiO_4$) to zirconia (ZrO_2) and silica (SiO_2); this is usually associated with the formation of closed pores, which reduces the density. As for HB00Z sample, the decrease in density is due to the formation of secondary millite from silica and alumina obtained from boehmite. Before reaction between these compounds, a mixture of three phases i.e. primary mullite, silica, and

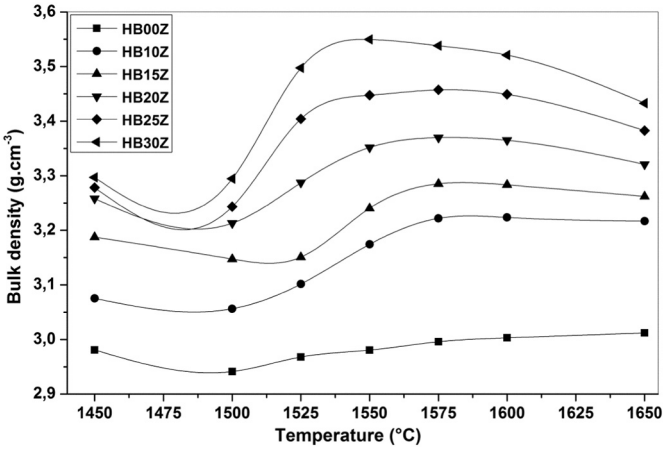

Fig. 7. Density of samples as a function of sintering temperature.

alumina was present, this mixture has a density higher than the mixture from which secondary mullite forms. In addition, the formation of closed pores affects the density. In the temperature range 1500 to 1600 °C, the increase in density is attributed to the increase in volume fraction of mullite and the decrease in the volume fraction of pores. Above 1600 °C, a small decrease in the density of samples containing higher than 15% ZrO_2 was observed. This is due to the fact that mullite grains had elongated shape and their growth, at relatively high temperatures, leaves behind closed pores which reduces the density.

Typical SEM images of surfaces of fractured HB00Z and HB20Z samples, sintered at 1600 °C for 2 h, are presented in Fig. 8. These micrographs support the results obtained from TDA, XRD, and dilatometry experiments, which confirmed the formation of only mullite phase in the halloysite–boehmite mixture and the presence of both mullite and zirconia in halloysite–boehmite–zirconia mixtures. The following can be concluded from the analysis of the microstructures: (i) both HB00Z and HB20Z samples had uniform microstructure with uniform distribution of small pores, (ii) the volume fraction of pores is higher in the HB20Z sample compared to HB00Z sample, (iii) the HB20Z sample showed uniform distribution of inter-granular ZrO_2 particles as indicated by white arrows in Fig. 8(b), and (iv) mullite phase had relatively large average grain size and less elongated shape in HB20Z compared to HB00Z sample.

3.4. Hardness and coefficient of linear thermal expansion

Hardness and coefficient of linear thermal expansion of samples, sintered at 1600 °C for 2 h, are presented in Fig 9(a) and (b), respectively. The HB00Z sample had a hardness of 11.3 GPa. The addition of 10 wt% zirconia to HB00Z sample increased its hardness to 13.5 GPa (an increase of 19.47%). A further increase in zirconia content up to 30% decreased the hardness to 12 GPa. However, the hardness of composites remained higher than the hardness of the HB00Z sample. The improvement in the hardness of mullite-zirconia composites could be attributed to the presence of the zirconia hard phase. The change in hardness followed the trend observed, in some ceramic based composites, by some researchers who investigated the influence of the addition of SiC on alumina and found that the hardness increased with an increase in SiC content up to 5 wt% (Saheb and Mohammad, 2016; Dong et al., 2009), 7.5 vol% (Ghadami et al., 2016), and 10 vol% (Johnson et al., 2014), then decreased with further increase in the SiC content. The hardness values between 12 and 13.5 GPa obtained for mullite-zirconia composites produced by reaction sintering Algerian halloysite with boehmite and zirconia at 1600 °C for 2 h, are slightly higher than the hardness values of composites obtained by reaction sintering (Ashrafi et al., 2015), or other processing methods such as plasma fusing of sillimanite and zircon in the presence

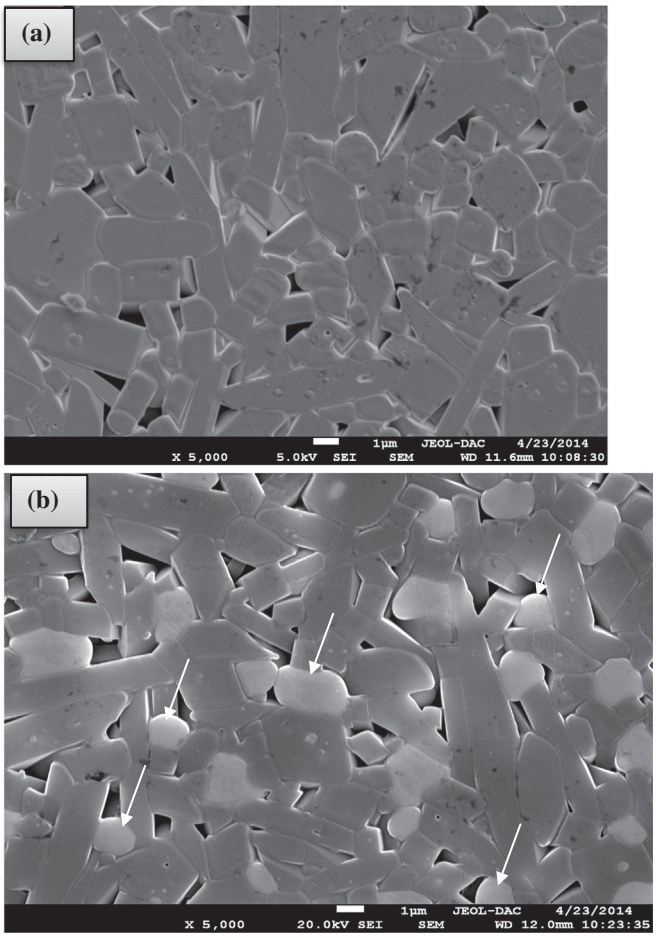

Fig. 8. SEM images of surfaces of fractured samples sintered at 1600 °C for 2 h (a) HB00Z and (b) HB20Z.

of magnesia (Prusty et al., 2012), and slip casting (Garrido et al., 2006). Ashrafi et al. (2015) obtained a hardness value of 11.1 GPa for mullite-zirconia composite produced by 60 h of mechanical activation and reaction sintering of zircon-alumina mixture at 1400 °C for 2 h. Prusty et al. (2012) obtained a hardness value between 10.8 and 11.8 GPa for mullite-zirconia composites processed by plasma fusing of sillimanite and zircon in the presence of magnesia. Garrido et al. (2006) reported a hardness value of ~9 to 12 GPa for mullite-zirconia composites obtained by slip casting.

The change in the coefficient of linear thermal expansion of zirconia containing samples, sintered at 1600 °C for 2 h, is illustrated in Fig. 9(b). The samples were heated from room temperature to 1600 °C using a heating rate of 5 °C/min, and then cooled to room temperature using the same rate. During heating the zirconia changed from tetragonal to monoclinic structure at around 1100 °C, and the change reverted during cooling at around 700 °C. The transformation was clear for HB20Z and HB30Z samples compared to HB10Z samples. The values of coefficient of linear thermal expansion of samples at different temperature ranges are summarized in Table 2. Samples containing 10 and 20% of zirconia had high fraction of the tetragonal phase, therefore their coefficient of linear thermal expansion values were close to that of tetragonal zirconia i.e. $10 \times 10^{-6}\,K^{-1}$ (Claussen and Jahn, 1980; Zender et al., 1990). For the temperature range between 200 and 1500 °C, the coefficient of linear thermal expansion varied between $9.056 \times 10^{-6}\,K^{-1}$ for the HB10Z sample to $8.4256 \times 10^{-6}\,K^{-1}$ for the HB20Z sample. As for the HB30Z sample which contained high fraction of the monoclinic phase, its coefficient of linear thermal expansion, between 200 and 1500 °C, was $7.5725 \times 10^{-6}\,K^{-1}$, which is close to that of monoclinic zirconia i.e.

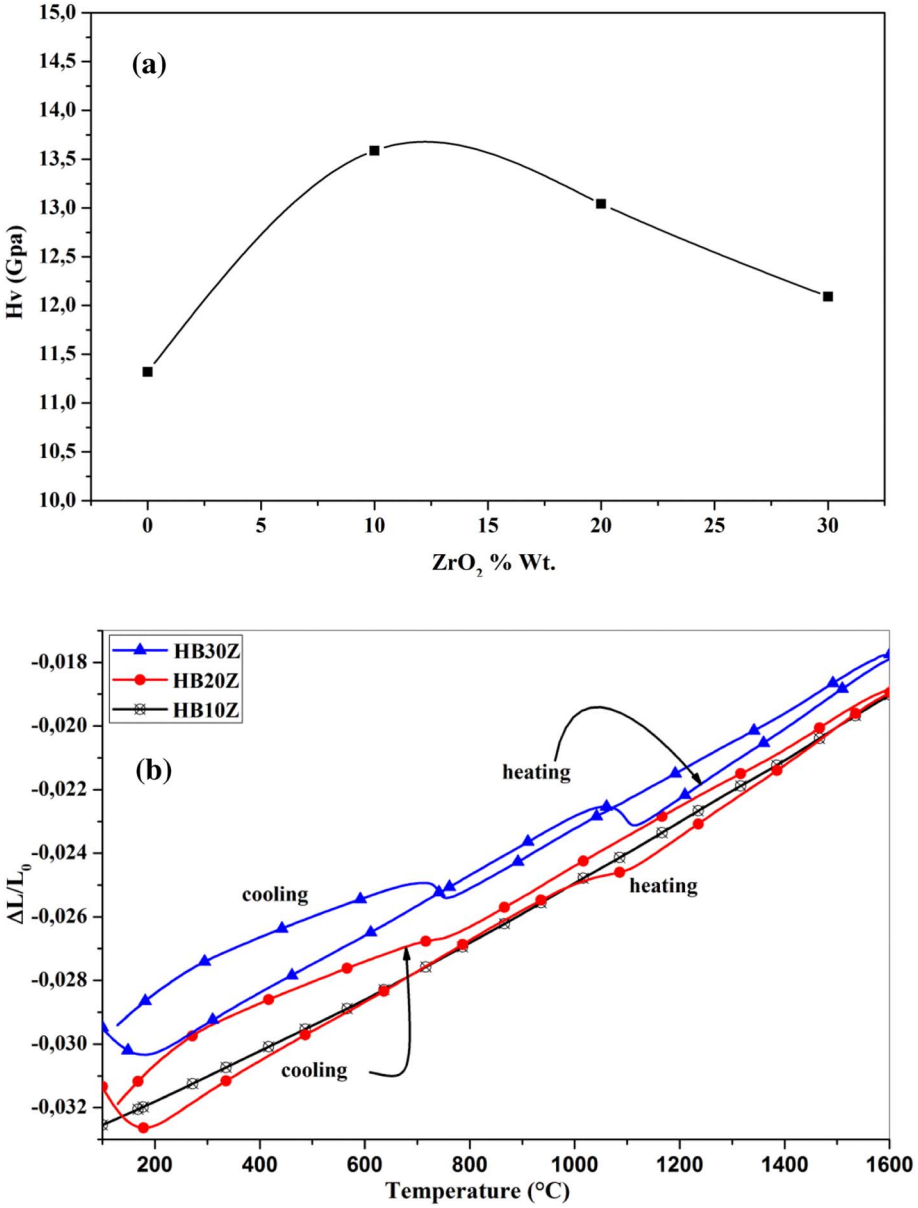

Fig. 9. (a) Vickers hardness and (b) coefficient of linear thermal expansion of composites sintered at 1600 °C for 2 h.

Table 2
Linear thermal expansion coefficient (α) of samples sintered at 1600 °C for 2 h.

Samples	Temperature range (°C)	$\alpha \times 10^{-6} K^{-1}$
KB10Z	200–1500	9,0560
	200–1200	8,7901
	200–1000	8,5882
	200–900	8,4372
KB20Z	200–1500	8,4256
	200–1200	8,1267
	200–1000	7,8170
	200–900	7,5349
KB30Z	200–1500	7,5725
	200–1200	6,9968
	200–1000	6,4861
	200–900	6,0367

$6 \times 10^{-6} K^{-1}$ (Claussen and Jahn, 1980; Zender et al., 1990). The values of the coefficient of linear thermal expansion of the developed composites are comparable with reported values, between 5.2 and $7.2 \times 10^{-6} K^{-1}$, for mullite-zirconia composites (Barin and Knacke, 1973).

4. Conclusion

Low-cost mullite-ZrO_2 composites were produced by reaction sintering Algerian halloysite with boehmite and zirconia. Phase transformations and sintering behavior of the synthesized materials were characterized using DTA/TG, dilatometry, and high temperature X-ray diffraction. The hardness and coefficient of linear thermal expansion of the developed materials were evaluated. Algerian halloysite was found suitable material for the synthesis of low-cost mullite based composites. All prepared samples exhibited same phase transformations, which ended with the formation of monolithic mullite in halloysite-boehmite mixture and mullite-zirconia composites in halloysite-boehmite-zirconia mixture. The composite materials showed higher values of hardness and coefficient of linear thermal expansion compared with monolithic mullite. The HB10Z composite possessed the highest hardness value of 13.5 GPa. The HB30Z composite possessed the lowest value of linear coefficient of thermal expansion of $7.5725 \times 10^{-6} K^{-1}$ between 200 and 1500 °C.

Acknowledgments

The authors are grateful to the department of physics, University Mohamed Boudiaf, M'sila, Algeria.

References

Alves, H.P., Silva, J.B., Campos, L.F., Torres, S.M., Dutra, R.P., Macedo, D.A., 2016. Preparation of mullite based ceramics from clay–kaolin waste mixtures. Ceram. Int. 42 (16), 19086–19090.
Alves, H.P., Junior, R.A., Campos, L.F., Dutra, R.P., Grilo, J.P., Loureiro, F.J., Macedo, D.A., 2017. Structural study of mullite based ceramics derived from a mica-rich kaolin waste. Ceram. Int. 43 (4), 3919–3922.
Ashrafi, H., Emadi, R., Foroushani, R.Z., 2015. Synthesis and characterization of mullite–zirconia nanostructured composite by combined mechanical activation and reaction sintering. Adv. Powder Technol. 26 (5), 1452–1457.
Aydın, H., Gören, R., 2016. Effect of colemanite on properties of traditional mullite zirconia composite. Cogent Eng. 3 (1), 1209809.
Barin, I., Knacke, O., 1973. Thermochemical Properties of Inorganic Substances. Springer.
Belhouchet, H., Hamidouche, M., Bouaouadja, N., Garnier, V., Fantozzi, G., 2007. Elaboration and microstructural characterization of a mullite-zirconia composite obtained by reaction sintering. Ann. Chim. Sci. Mater. 605–614.
Belhouchet, H., Hamidouche, M., Bouaouadja, N., Garnier, V., Fantozzi, G., 2009. Elaboration and characterization of mullite–zirconia composites from gibbsite, boehmite and zircon. Ceram. Silikaty 53 (3), 205–210.
Belkassa, K., Bessaha, F., Marouf-Khelifa, K., Batonneau-Gener, I., Comparot, J.D., Khelifa, A., 2013. Physicochemical and adsorptive properties of a heat-treated and acid-leached Algerian halloysite. Colloids Surf. A Physicochem. Eng. Asp. 421, 26–33.
Bessaha, F., Marouf-Khelifa, K., Batonneau-Gener, I., Khelifa, A., 2016. Characterization and application of heat-treated and acid-leached halloysites in the removal of malachite green: adsorption, desorption, and regeneration studies. Desalin. Water Treat. 57 (31), 14609–14621.
Bhattacharya, I.N., Das, S.C., Mukherjee, P.S., Paul, S., Mitra, & P.K., 2004. Thermal decomposition of precipitated fine aluminium trihydroxide. Scand. J. Metall. 33 (4), 211–219.
Brindley, G.W., Choe, J.O., 1961. The reaction series, gibbsite → chi alumina → kappa alumina → corundum. Am. Mineral. 46 (7–8), 771–785.
Brindley, G.W., Lemaitre, J., 1987. Thermal oxidation and reduction reactions of clay minerals: in Chemistry of Clays and Clay Minerals. In: Newman, A.C.D. (Ed.), Longman Scientific and Technical (Essex), Mineralogical Society, London, pp. 319–370.
Candela, L., Perlmutter, D.D., 1986. Pore structure and kinetics of the thermal decomposition of Al $(OH)_3$. AICHE J. 32 (9), 1532–1545.
Candela, L., Perlmutter, D.D., 1992. Kinetics of boehmite formation by thermal decomposition of gibbsite. Ind. Eng. Chem. Res. 31 (3), 694–700.
Cesteros, Y., Salagre, P., Medina, F., Sueiras, J.E., 1999. Several factors affecting faster rates of gibbsite formation. Chem. Mater. 11 (1), 123–129.
Chandra, D., Das, G., Maitra, S., 2015. Comparison of the role of MgO and CaO additives on the microstructures of reaction-sintered zirconia–mullite composite. Int. J. Appl. Ceram. Technol. 12 (4), 771–782.
Chen, Y.F., Wang, M.C., Hon, M.H., 2004. Phase transformation and growth of mullite in kaolin ceramics. J. Eur. Ceram. Soc. 24 (8), 2389–2397.
Churchman, G.J., Pasbakhsh, P., Hillier, S., 2016. The rise and rise of halloysite. Clay Miner. 51 (3), 303–308.
Claussen, N., Jahn, J., 1980. Mechanical properties of sintered, in situ-reacted mullite-zirconia composites. J. Am. Ceram. Soc. 63 (3–4), 228–229.
Das, K., Mukherjee, B., Banerjee, G., 1998. Effect of yttria on mechanical and microstructural properties of reaction sintered mullite-zirconia composites. J. Eur. Ceram. Soc. 18 (12), 1771–1777.
Day, M.K., Hill, V.J., 1953. The thermal transformations of the aluminas and their hydrates. J. Phys. Chem. 57 (9), 946–950.
Digne, M., Sautet, P., Raybaud, P., Toulhoat, H., Artacho, E., 2002. Structure and stability of aluminum hydroxides: a theoretical study. J. Phys. Chem. B 106 (20), 5155–5162.
Dong, Y.L., Xu, F.M., Shi, X.L., Zhang, C., Zhang, Z.J., Yang, J.M., Tan, Y., 2009. Fabrication and mechanical properties of nano-/micro-sized Al_2O_3/SiC composites. Mater. Sci. Eng. A 504 (1), 49–54.
Ebadzadeh, T., 2005. Porous mullite-ZrO_2 composites from reaction sintering of zircon and aluminum. Ceram. Int. 31 (8), 1091–1095.
Filho, R.W.N.D., Rocha, G.A., Montes, C.R., Vieira-Coelho, A.C., 2016. Synthesis and characterization of boehmites obtained from gibbsite in presence of different environments. Mater. Res. 19 (3), 659–668.
Garrido, L.B., Aglietti, E.F., Martorello, L., Camerucci, M.A., Cavalieri, A.L., 2006. Hardness and fracture toughness of mullite-zirconia composites obtained by slip casting. Mater. Sci. Eng. A 419 (1), 290–296.
Ghadami, S., Baharvandi, H.R., Ghadami, F., 2016. Influence of the vol% SiC on properties of pressureless Al_2O_3/SiC nanocomposites. J. Compos. Mater. 50 (10), 1367–1375.
Gitzen, W.H., 1970. Alumina as a Ceramic Material. ACS, Columbus, Ohio (Chapter 1).
Harabi, A., Zenikheri, F., Boudaira, B., Bouzerara, F., Guechi, A., Foughali, L., 2014. A new and economic approach to fabricate resistant porous membrane supports using kaolin and $CaCO_3$. J. Eur. Ceram. Soc. 34 (5), 1329–1340.
Heraiz, M., Sahnoune, F., Belhouchet, H., Saheb, N., 2013. Synthesis of Al_2O_3 containing mullite from Algerian kaolin and boehmite. J. Optoelectron. Adv. Mater. 15 (11 − 12), 1263–1267.
Johnson, O.T., Rokebrand, P., Sigalas, I., 2014. In Proceedings of the World Congress on Engineering. Microstructure and Properties of Al_2O_3–SiC Nanomaterials, vol. 2 International Association of Engineers, London, U.K.
Joussein, E., Petit, S., Churchman, J., Theng, B., Righi, D., Delvaux, B., 2005. Halloysite clay minerals–a review. Clay Miner. 40 (4), 383–426.
Joussein, E., Petit, S., Fialips, C.I., Vieillard, P., Righi, D., 2006. Differences in the dehydration-rehydration behavior of halloysites: New evidence and interpretations. Clays Clay Miner. 54, 473–484.
Kadi, S., Lellou, S., Marouf-Khelifa, K., Schott, J., Gener-Batonneau, I., Khelifa, A., 2012. Preparation, characterisation and application of thermally treated Algerian halloysite. Microporous Mesoporous Mater. 158, 47–54.
Lin, Y.J., 1999. Reaction synthesis of mullite-zirconia from mixtures of alumina, silica, and 3 mol% yttria-zirconia powders. J. Mater. Res. 14 (03), 916–924.
Liu, K.C., Thomas, G., Caballero, A., Moya, J.S., Aza, S., 1994. Time-temperature-transformation curves for kaolinite-α-alumina. J. Am. Ceram. Soc. 77 (6), 1545–1552.
Mahrez, N., Bendenia, S., Marouf-Khelifa, K., Batonneau-Gener, I., Khelifa, A., 2015. Improving of the adsorption capacity of halloysite nanotubes intercalated with dimethyl sulfoxide. Compos. Interfaces 22 (6), 403–417.
Manfredini, T., Manuskova, M., 2012. Natural Raw Materials in "Traditional" Ceramic Manufacturing. J. Univ. Chem. Technol. Metall. 47 (4), 465–470.
Medeiros, S.G., Dutra, R.P.S., Grilo, J.P.F., Martinelli, A.E., Paskocimas, C.A., Macedo, D.A., 2016. Preparation of low-cost alumina-mullite composites via reactive sintering between a kaolinite clay from Paraíba and aluminum hydroxide. Cerâmica 62 (363), 266–271.
Mellouk, S., Cherifi, S., Sassi, M., Marouf-Khelifa, K., Bengueddach, A., Schott, J., Khelifa, A., 2009. Intercalation of halloysite from Djebel Debagh (Algeria) and adsorption of copper ions. Appl. Clay Sci. 44 (3), 230–236.
Mercury, J.M., Pena, P., Aza, A.H., Sheptyakov, D., Turillas, X., 2005. On the decomposition of synthetic gibbsite studied by neutron thermodiffractometry. J. Am. Ceram. Soc. 89 (12), 3728–3733.
Okada, K., Otsuka, N., Ossaka, J., 1986. Characterization of spinel phase formed in the kaolin-mullite thermal sequence. J. Am. Ceram. Soc. 69, C-251–C-253.
Öztürk, C., Tür, Y.K., 2007. Processing and mechanical properties of textured mullite/zirconia composites. J. Eur. Ceram. Soc. 27 (2), 1463–1467.
Park, H.C., Yang, T.Y., Yoon, S.Y., Stevens, R., 2005. Preparation of zirconia–mullite composites by an infiltration route. Mater. Sci. Eng. A 405 (1), 233–238.
Pask, J.A., Tomsia, A.P., 1991. Formation of mullite from sol-gel mixtures and kaolinite. J. Am. Ceram. Soc. 74 (10), 2367–2373.
Prusty, S., Mishra, D.K., Mohapatra, B.K., Singh, S.K., 2012. Effect of MgO in the microstructure formation of zirconia mullite composites from sillimanite and zircon. Ceram. Int. 38 (3), 2363–2368.
Rajabi, L., Derakhshan, A.A., 2010. Room temperature synthesis of boehmite and crystallization of nanoparticles: effect of concentration and ultrasound. Sci. Adv. Mater. 2 (2), 163–172.
Ramani, S.V., Subbarao, E.C., Gowhale, K.V.G.M., 1969. Kinetics of zircon synthesis. J. Am. Ceram. Soc. 52 (11), 619–623.
Rendtorff, N.M., Garrido, L.B., Aglietti, E.F., 2008. Thermal shock behavior of dense mullite–zirconia composites obtained by two processing routes. Ceram. Int. 34 (8), 2017–2024.
Rezaie, H.R., Rainforth, W.M., Lee, W.E., 1999. Fabrication and mechanical properties of SiC platelet reinforced mullite matrix composites. J. Eur. Ceram. Soc. 19 (9), 1777–1787.
Saheb, N., Mohammad, K., 2016. Microstructure and mechanical properties of spark plasma sintered Al_2O_3-SiC-CNTs hybrid nanocomposites. Ceram. Int. 42 (10), 12330–12340.
Sahnoune, F., Chegaar, M., Saheb, N., Goeuriot, P., Valdivieso, F., 2008a. Algerian kaolinite used for mullite formation. Appl. Clay Sci. 38 (3), 304–310.
Sahnoune, F., Chegaar, M., Saheb, N., Goeuriot, P., Valdivieso, F., 2008b. Differential thermal analysis of mullite formation from Algerian kaolin. Adv. Appl. Ceram. 107 (1), 9–13.
Sahnoune, F., Saheb, N., Chegaar, M., Goeuriot, P., 2010. Materials Science Forum. Microstructure and Sintering Behavior of Mullite-Zirconia Composites, vol. 638. Trans Tech Publicationspp. 979–984.
Sahnoune, F., Belhouchet, H., Saheb, N., Heraiz, M., Chegaar, M., Goeuriot, P., 2011. Phase transformation and sintering behaviour of mullite and mullite–zirconia composite materials. Adv. Appl. Ceram. 110 (3), 175–180.
Schneider, H., Okada, K., Pask, J., 1994. Mullite and Mullite Ceramics. John Wiley & Sons, New York, pp. 169–176.
Shi, Y., Huang, X., Yan, D., 1997. Fabrication of hot-pressed zircon ceramics: mechanical properties and microstructure. Ceram. Int. 23 (5), 457–462.
Smith, M.E., Neal, G., Trigg, M.B., Drennan, J., 1993. Structural characterization of the thermal transformation of halloysite by solid-state NMR. Appl. Magn. Reson. 4, 157–170.
Sonuparlak, B., Sarikaya, M., Aksay, I.A., 1987. Spinel phase formation during the 980°C exothermic reaction in the kaolinite-to-mullite reaction series. J. Am. Ceram. Soc. 70 (11), 837–842.
Tan, D., Yuan, P., Annabi-Bergaya, F., Dong, F., Liu, D., He, H., 2015. A comparative study of tubular halloysite and platy kaolinite as carriers for the loading and release of the herbicide amitrole. Appl. Clay Sci. 114, 190–196.
Tan, D., Yuan, P., Liu, D., Du, P., 2016. Surface modifications of halloysite (chapter 8). In nanosized tubular clay minerals halloysite and imogolite. Part II: structure and properties of Nanosized tubular clay minerals, edited by Peng Yuan, Antoine thill and Feaïza Bergaya. Developments in Clay Science 7, 167–201.
Torrecillas, R., Moya, J.S., De Aza, S., Gros, H., Fantozzi, G., 1993. Microstructure and mechanical properties of mullite-zirconia reaction-sintered composites. Acta Metall.

Mater. 41 (6), 1647–1652.
Wang, J.Q., Liu, J.L., Liu, X.Y., Qiao, M.H., Pei, Y., Fan, K.N., 2009. Hydrothermal transformation of bayerite to boehmite. Sci. Adv. Mater. 1 (1), 77–85.
Wefers, K., Misra, C., 1987. Oxides and Hydroxides of Aluminum. ALCOA Laboratories, Pittsburgh.
Yangyun, S., Brook, R.J., 1985. Preparation of zirconia-toughened ceramics by reaction sintering. Sci. Sinter. 17 (1), 35–47.
Yuan, Peng, Tan, Daoyong, Aannabi-Bergaya, Faïza, Yan, Wenchang, Fan, Mingde, Liu, Dong, He, Hongping, 2012. Changes in structure, morphology, porosity, and surface activity of mesoporous halloysite nanotubes under heating. Clay Clay Miner. 60 (6), 561–573.
Yuan, P., Tan, D., Annabi-Bergaya, F., 2015. Properties and applications of halloysite nanotubes: recent research advances and future prospects. Appl. Clay Sci. 112, 75–93.
Zender, H.H., Leistner, H., Searle, H.R., 1990. ZrO_2 materials for application in the ceramics industry. Interceram 39 (6), 33–36.